Wave form of de Haas–van Alphen oscillations in a two-dimensional metal

M. A. Itskovsky and T. Maniv
Department of Chemistry, Technion–Israel Institute of Technology, Haifa 32000, Israel

I. D. Vagner
Grenoble High Magnetic Fields Laboratory, MPI-FKF and CNRS, BP 166X, F-38042, Grenoble Cedex 9, France
(Received 8 December 1999; revised manuscript received 7 February 2000)

The effect of thermodynamical equilibrium transfer of electrons between closed (Landau) orbits and magnetic field independent states near the Fermi surface on the magnetoquantum oscillations in quasi-two-dimensional (2D) metals is investigated. The general relationship between magnetization and chemical potential oscillations in such a model is derived, and a variety of wave forms are obtained in the entire temperature–magnetic field region. It is shown quite generally that such an electron transfer suppresses the chemical potential oscillations, whereas the magnetization amplitude remains unchanged. A specific model of the relevant band structure in which the field independent (or reservoir) states correspond to quasiplanar energy surfaces is considered in detail. In this model, the chemical potential oscillations diminish when the bottom of the subband with the quasiplanar energy surfaces nearly coincides with the Fermi energy, and the corresponding one-dimensional van Hove singularity dominates the electron transfer. Similarly, the chemical potential may be pinned due to electrons in localized states near the Fermi energy. In both cases the de Haas–van Alphen oscillations are shown to have an inverse-sawtooth shape at sufficiently low temperatures. In the more common situation when the Fermi energy is relatively far from any sharp peak of the reservoir density of states, the wave form of the magnetization oscillations is symmetrized at all temperatures. All shapes of magnetization oscillations observed in the organic quasi-2D metals of the (BEDT-TTF)$_2X$ type, from the rare sawtooth and inverse-sawtooth to the usual symmetrical ones, can be accounted for by this model.

I. INTRODUCTION

The phenomenon of magnetoquantum oscillations in Fermi liquids under high quantizing magnetic field [which is the essence of the de Haas–van Alphen (dHvA) effect] provides a powerful tool for investigating the Fermi surfaces of three-dimensional[1] (3D) and two-dimensional[2] (2D) metals.

The main attention has been paid so far to the temperature dependence of the dHvA amplitude from which the cyclotron masses can be extracted by applying the standard analysis[1,2] based on the Lifshitz-Kosevich formulas.[3] Only a little work has been devoted to the observation and interpretation of the wave form (shape) of the magnetoquantum oscillations. In 3D metals the shape of the oscillations is quite smooth and symmetrical. In 2D metals the sawtooth oscillations predicted by the theory[4] have been observed in only a few experiments.[5,6] Asymmetrical Shubnikov–de Haas and dHvA oscillations were also observed recently by Brooks *et al.* in 2D organic metals,[7,8] in which the variety of wave forms was attributed to the influence of the quasiplanar sheets of the Fermi surface.

The magnetoquantum oscillations in 2D electron systems, such as the conduction electrons in 2D organic metals,[2] are usually considered in two extreme limits: (1) the limit of a fixed number of electrons filling a discrete spectrum of (Landau) levels (LLs), which constitutes a canonical ensemble of electrons,[9] or (2) the limit of fixed chemical potential, which can be represented by a grand canonical ensemble. In the latter case it is implicitly assumed that some electrons can also occupy field independent energy levels which pin the chemical potential.[10] In both cases an extreme sawtooth (or inverse-sawtooth) shape of magnetic oscillations at $T \to 0$ is obtained, so that the only difference between the two cases is the sign of the slopes of the linear parts.[1,10,4] Usually, however, neither limit is realized, since on a macroscopic time scale the electrons can be transferred to states that are not influenced by the magnetic field. A concrete example of such field independent states is the continuous subband corresponding to the open, quasiplanar parts of the Fermi surface [quasi-one-dimensional (1D) sheets] found in some of the (BEDT-TTF)$_2X$ type compounds,[2] impurity (defect) local states, or the localized intercalant states in layered intercalation compounds,[11] etc. Consequently, as a result of electron transfer between the two subsets of energy levels, the number of electrons filling both the Landau levels and the field independent levels changes on varying the magnetic field. This electron transfer is a purely thermodynamical equilibrium phenomenon, since it is associated exclusively with the chemical potential oscillations. As will be shown later, this transfer is most effective for field independent levels situated near the Fermi energy.

For a model of a Fermi surface consisting of a quasicylindrical and a quasiplanar sheet the degree of this transfer depends on the energy barrier and the gap in momentum space between the cylinder and the quasiplanar sheets.[12] The influence of such an electron transfer on magnetoquantum oscillations in quasi-2D organic conductors was considered analytically in Ref. 12 and numerically in Ref. 13. A rather similar model, but for two coupled closed pockets of electrons, was considered by Alexandrov and Bratkovsky.[14]

Here we first address the general problem of equilibrium transfer of electrons between a spectrum of Landau levels

and a field independent energy spectrum, without specifying the transfer mechanism, in order to determine the conditions for observation of the various wave forms of dHvA oscillations in 2D metals. We will consider the relations between magnetization and chemical potential oscillations in such a general situation.

We shall then consider the case of a quasi-2D organic metal having disconnected closed and open sheets of the Fermi surface.[2,5–8] We find that the parameters determining the transfer of electrons between these sheets are the energy difference between the bottoms of the corresponding quasi-2D and 1D subbands as well as the corresponding effective masses. In the special case when the bottom of the 1D subband nearly coincides with the Fermi energy, and for $T \rightarrow 0$, the van Hove singularity at the bottom of the 1D subband pins the chemical potential and thus leads to an inverse-sawtooth shape of the oscillations at sufficiently low temperature. In the more common situation when the bottom of the 1D subband is not very close to the Fermi energy, one finds the usual quasisymmetrical wave form of oscillations observed in organic metals. A complete depinning of the chemical potential can occur when all kinds of field independent states are situated far away from the Fermi energy. This situation corresponds to the rarely observed sawtooth wave form of oscillations at ultralow temperature.

The paper is organized as follows. In Sec. II a general relationship between the chemical potential and magnetization oscillations is derived for a model consisting of field dependent (Landau) levels and a field independent energy spectrum near the Fermi energy. In Sec. III an exact parametrical method of calculating the wave form of the magnetoquantum oscillations in a 2D metal is presented. We consider the chemical potential oscillations in our model and determine the conditions under which the chemical potential oscillations are suppressed. The shape of magnetization oscillations is studied in detail. In Sec. IV available experimental data concerning the wave form of magnetization in 2D organic metals are compared with the relevant band structure of some quasi-2D organic compounds of the $(BEDT\text{-}TTF)_2X$ type.

II. GENERAL CONSIDERATIONS

We consider a model of a quasi-2D metal under high quantizing magnetic field having an energy subband near the Fermi energy represented by quasicylindrical energy surfaces. Generally there is also a ''reservoir'' of electrons filling extended states (e.g., corresponding to open energy sheets) or localized states (due to impurities or other defects) not influenced by the magnetic field.

More specifically, the band structure of some of the $(BEDT\text{-}TTF)_2X$ type organic conductors serves as a prototype of such a quasi-2D metal. In these compounds the conduction electron energy dispersion along the anisotropic axis (i.e., along k_z) is negligible in comparison with the dispersion in the plane perpendicular to k_z, so that the bandwidth in the k_z direction, $\Delta_z \ll \varepsilon_F$, where ε_F is the Fermi energy. In addition to the corresponding quasicylindrical energy sheet, the typical Fermi surface of these compounds consists of a disconnected quasiplanar sheet arising from an additional upper energy band. These materials also contain some impurity (defect) levels.

In high enough magnetic fields the quasicylindrical energy surfaces will be quantized and electrons will be moving on closed (usually holelike) orbits. The quasiplanar energy sheets form a continuous band with electrons moving on open orbits under the influence of an external magnetic field.

We assume magnetic fields at which the tunneling probability of magnetic breakdown between closed and open orbits is negligible, $P_{tun} \sim \exp(-B_{br}/B) \ll 1$ (B_{br} is the breakdown magnetic field[1]). Under these circumstances the tunneling rate is much smaller than the characteristic cyclotron frequency and there is no influence on the dHvA frequency. However, the small electron transfer between the cylindrical and planar sheets [and/or impurity (defect) levels] can significantly influence the thermodynamical equilibrium between the two electronic subsystems.

Let us consider now the general relationship between magnetization and chemical potential oscillations in the model described above. To describe the subsystem of electrons in the closed orbits we use the expression for the thermodynamical potential of 2D electron gas in high magnetic field:[3,15]

$$\frac{\Omega_{\mathrm{LL}}(B,\zeta)/V}{A} = -\frac{B}{\beta}\sum_{n=0} \ln(1+\exp\{[\zeta-\varepsilon_n(B)]\beta\}), \tag{1}$$

where $A \equiv 2\cos\Theta/c^*\phi_0, \phi_0 = hc/e$ is the flux quantum, $\beta \equiv 1/k_B T$, c^* is the lattice constant in the anisotropic direction, and Θ is the angle between the anisotropic axis $\mathbf{c}^*$ and the magnetic induction vector $\mathbf{B}$.

Note that in writing this expression the magnetic field is assumed to be high enough such that the bandwidth Δ_z of the energy dispersion in the k_z direction can be neglected in comparison with the cyclotron energy. We also neglect spin splitting of the Landau levels. This is justified for special angles[16] Θ_{sp} for which $G = G_0/\cos\Theta_{sp} = I$ [I is an integer number, $G_0 \equiv (g/2)m_{c0}/m_e$, g is the electron g factor, m_{c0} is the cyclotron mass in the $\Theta = 0$ direction, and m_e is the electron mass] or for electron systems with negligibly small g factor, $g \ll 1$.

The corresponding energy spectrum (Landau levels) is

$$\varepsilon_n(B) = \hbar\omega_c(B)(n+1/2), \quad n = 0,1,2,\ldots, \tag{2}$$

where $\omega_c(B) = eB/m_c c$ is the cyclotron frequency, $m_c = m_{c0}/\cos\Theta$ is the cyclotron mass, m_{c0} is the cyclotron mass at $\Theta = 0$. The intersections of Landau levels, Eq. (2), with the Fermi energy on varying the magnetic field strength lead to the magnetoquantum oscillations. Let us define discrete magnetic field values $B_{\bar{n}}$ and $B_{\bar{n}+1}$ so that ε_F is situated at equal distance from the two successive levels with fixed quantum numbers $\bar{n}$ and $\bar{n}-1$ and $\bar{n}$ and $\bar{n}+1$, respectively (see Fig. 1),

$$[\varepsilon_{\bar{n}}(B_{\bar{n}}) + \varepsilon_{\bar{n}-1}(B_{\bar{n}})]/2 = \varepsilon_F. \tag{3}$$

Rearranging the summation in the thermodynamical potential [Eq. (1)] over levels below and above the level with fixed quantum number $\bar{n}$ (see Fig. 1), we have

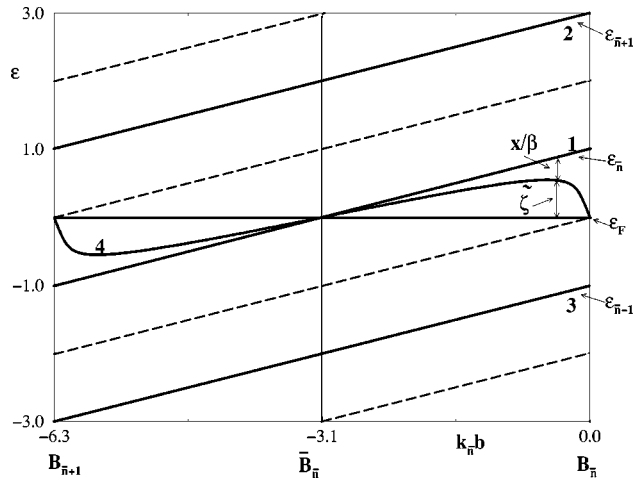

FIG. 1. Landau levels around the Fermi energy giving the main contribution to the chemical potential and magnetization oscillations in a 2D metal in a separated period of magnetic field. This period, situated on the left-hand side relative to the magnetic field B_n^- (which corresponds to the crossing by the middle curve between levels of the Fermi energy), is in the range of magnetic fields $B_{n+1}^- \leqslant B \leqslant B_n^-$ or equivalently $-2b_n^- \leqslant b = B - B_n^- \leqslant 0$, where $b_n^- = B_{n+1}^- B_n^-/2F$ is the half period, F is the fundamental frequency of oscillations relative to the inverse magnetic field $1/B$, and $k_n^- \equiv \pi/b_n^-$ is the fundamental cyclic frequency relative to the magnetic field difference $b = B - B_n^-$. The chemical potential oscillations (curve 4) are drawn according to the parametric Eqs. (25) and (26) for parameters $Q = 20$, $c_R = 0.1$. Energies, measured from ε_F, are given in units of $\hbar\omega_c/2$. Curves 1, 2, and 3 correspond to the energy levels ε_n^-, ε_{n+1}^-, and ε_{n-1}^-. The midpoints between energy levels are shown by the dashed lines. Magnetic fields corresponding to the edges of the separated period are B_{n+1}^- and B_n^-. The center of the period, $\bar{B}_n^-$, where separated level ε_n^- crosses ε_F, is shown by the thin solid line. Note the symmetry of the level dispositions relative to the Fermi energy at magnetic fields B_{n+1}^-, $\bar{B}_n^-$ and B_n^-. $\tilde{\zeta}(b) = \zeta(B) - \varepsilon_F$ is the oscillating part of the chemical potential $\zeta(B)$, and $x(b)/\beta \equiv \varepsilon_n^-(B) - \zeta(B)$ is the energy difference between the separated level crossing the chemical potential inside the period ε_n^- and the oscillating chemical potential $\zeta(B)$ [$x(b, \tilde{\zeta})$ is the parametric variable].

$$\sum_{n=0} \ln\{1+\exp[(\zeta-\varepsilon_n)\beta]\}$$

$$= \beta \sum_{n=0}^{\bar{n}-1} (\zeta-\varepsilon_n) + \ln\{1+\exp[(\zeta-\varepsilon_n^-)\beta]\}$$

$$+ \sum_{n=0}^{\bar{n}-1} \ln\{1+\exp[(\varepsilon_n-\zeta)\beta]\}$$

$$+ \sum_{n=\bar{n}+1} \ln\{1+\exp[(\zeta-\varepsilon_n)\beta]\}. \quad (4)$$

Introducing the dimensionless parameters

$$x(B) \equiv [\varepsilon_n^-(B) - \zeta(B)]\beta \quad (5)$$

and

$$Q(B,T) \equiv \hbar\omega_c\beta \quad (6)$$

(see Fig. 1), the thermodynamical potential for electrons in the Landau levels can be written as

$$\frac{(\Omega_{\rm LL}/V)}{A} = -B\sum_{n=0}^{\bar{n}-1} (\zeta-\varepsilon_n) - \frac{B}{\beta} f(x,Q),$$

$$f(x,Q) \equiv \ln[1+\exp(-x)] + \sum_{k=1}^{\bar{n}} \ln[1+2\exp(-kQ)\cosh x + \exp(-2kQ)]. \quad (7)$$

Actually, only a few levels around the Fermi energy play an important role in determining the magnetoquantum oscillations. Therefore, in the representation of the thermodynamical potential, Eq. (7), the contributions of the levels with quantum numbers $n \geqslant (2\bar{n}+1)$ are omitted, since their contributions are negligibly small for $\bar{n} \gg 1$ relative to the remaining terms associated with the levels on both sides of the Fermi energy.

As discussed above, a collection of electrons filling states situated around the open parts of the Fermi surface, and/or localized states, may be regarded as a reservoir of carriers occupying a magnetic field independent spectrum. The electrons in this reservoir are in thermal equilibrium with electrons in the closed (quantized) orbits, and in this manner influence the quantum oscillations. If the spin splitting in the reservoir spectrum is also neglected the only magnetic field dependence remaining is through the oscillating chemical potential. Hence, since in this case the thermodynamical potential of the electronic reservoir is explicitly independent of the magnetic field (i.e., depends only implicitly through the chemical potential) it does not contribute directly to the magnetization, i.e., $\mathbf{M} = -[\partial(\Omega/V)/\partial\mathbf{B}]_\zeta = -[\partial(\Omega_{\rm LL}/V)/\partial\mathbf{B}]_\zeta$, where $\Omega = \Omega_{\rm LL}(B,\zeta) + \Omega_R(\zeta)$ is the total thermodynamic potential, and $\Omega_R(\zeta)$ is the thermodynamical potential of the reservoir.

Assuming a continuous reservoir spectrum, the corresponding thermodynamical potential can be written as

$$\Omega_R^{(cont)}/V = -(2/\beta)\sum_{\mathbf{k}} \ln\{1+\exp[(\zeta-\varepsilon_{\mathbf{k}})\beta]\}, \quad (8)$$

where $\varepsilon_{\mathbf{k}}$ is the energy dispersion law in the continuous subband. A similar expression can be written for a reservoir of localized impurity states.

The densities of electrons filling the Landau levels (LL) and the reservoir (R) spectrum, $n_{\rm LL}$ and n_R, respectively, are connected through

$$n_c = -\{\partial[(\Omega_{\rm LL}+\Omega_R)/V]/\partial\zeta\}_B = n_{\rm LL} + n_R, \quad (9)$$

where n_c is the total number density of electrons, which is constant in the magnetic field, $\Omega_R(\zeta) = \Omega_R^{(cont)}(\zeta) + \Omega_R^{(loc)}(\zeta)$, and $n_R = \{\partial\Omega_R/\partial\zeta\}_B$. Expanding the reservoir density $n_R(\zeta)$ in powers of the oscillating part of the chemical potential, $\tilde{\zeta}(B) = \zeta(B) - \varepsilon_F$,

$$n_R(\zeta) = n_R(\varepsilon_F) + n_R'(\varepsilon_F)\tilde{\zeta} + \tfrac{1}{2}n_R''(\varepsilon_F)\tilde{\zeta}^2 + \cdots,$$

$$n_R'(\varepsilon_F)\equiv\left(\frac{\partial n_R}{\partial\zeta}\right)_{\varepsilon_F},\quad n_R''(\varepsilon_F)\equiv\left(\frac{\partial^2 n_R}{\partial\zeta^2}\right)_{\varepsilon_F},\qquad(10)$$

and taking into account Eq. (7), the total density may be written as

$$n_c=AB[\bar{n}+g(x,Q)]+n_R(\varepsilon_F)+n_R'(\varepsilon_F)\tilde{\zeta}(B),$$

$$g(x,Q)=\frac{1}{1+\exp(x)}-\sum_{k=1}^{\bar{n}}\frac{\sinh x}{\cosh x+\cosh(kQ)}.\qquad(11)$$

up to first order in $\tilde{\zeta}$. Note that the chemical potential coincides with the Fermi energy at magnetic fields B_n^- and B_{n+1}^-, as well as at the field $\bar{B}_n^-$ where the fixed level ε_n^- in this period coincides with the Fermi energy (see Fig. 1). At these magnetic fields the LLs are arranged symmetrically relative to the Fermi energy (electron-hole symmetry), so that at the center of the period, where $x(\bar{B}_n^-)=0$, the function $g(0,Q)=1/2$, whereas at the right edge of the period, where $x(B_n^-)=Q/2$ the function $g(Q/2,Q)=0$ and at the left edge of the period, where $x(B_{n+1}^-)=-Q/2$, the function $g(-Q/2,Q)=1$. It is remarkable that these values of the function $g(x,Q)$ do not depend on the parameter Q: i.e., are independent of temperature for the magnetic field values B_{n+1}^- (left edge of the period), and $\bar{B}_n^-$ (center of the period), and B_n^- (right edge of the period).

From Eq. (11) it follows that the fundamental frequency of oscillations, F, can be determined by the relations

$$F=\frac{\varepsilon_F}{\mu_c}=\frac{n_c-n_R(\varepsilon_F)}{A},\quad \mu_c\equiv\frac{e\hbar}{m_c c}.\qquad(12)$$

The last equality constitutes the equation determining the Fermi energy ε_F as measured from the bottom of the 2D subband corresponding to the closed orbits (see Fig. 7 below).

The fixed quantum number $\bar{n}$ can be related to B_n^- by [Eq. (3)]

$$\bar{n}=\frac{\varepsilon_F}{\hbar\omega_c(B_n^-)}=\frac{F}{B_n^-},\qquad(13)$$

where in deriving the last equality the relation $\hbar\omega_c(B)=\mu_c B$ was used. Taking into account this relation we obtain from Eq. (11),

$$\frac{F}{B}-\frac{F}{B_n^-}=-\frac{b}{2b_n^-}=g(x,Q)+c_R\frac{\tilde{\zeta}(b)}{\hbar\omega_c(B)},\qquad(14)$$

where the reduced magnetic field b is defined with respect to B_n^-, i.e., $b=B-B_n^-$, and

$$c_R=\frac{n_R'\mu_c}{A}=\frac{\pi\hbar^2 c^*}{m_{c0}}n_R'\qquad(15)$$

is the parameter characterizing the strength of the electron transfer.

Note that $b_n^-=B_{n+1}^-B_n^-/2F=(B_n^2/2F)/(1+B_n^-/F)=\pi/k_n^-$ is the half period of the oscillation, where $k_n^-\equiv 2\pi F/B_{n+1}^-B_n^-$ is the fundamental frequency relative to the reduced magnetic field b. Note also that Eq. (14) holds in every quasiperiod $B_{n+1}^-\leqslant B\leqslant B_n^-$ (or $-2b_n^-\leqslant b\leqslant 0$), and that it is a valid approximation as long as $b_n^-\ll B_n^-$ [a factor $B_{n+1}^-/B\cong 1$ on the left-hand side of Eq. (14) is omitted].

If we retain in the series of Eq. (10) terms of higher than the first order in $\tilde{\zeta}$ we should use in Eq. (14), instead of the transfer parameter independent of chemical potential oscillations defined by Eq. (15), the transfer function $c_R(\tilde{\zeta})=(\pi\hbar c^*/m_{c0})[n_R'+(1/2)n_R''\tilde{\zeta}+\cdots]$. The additive terms in Eq. (14) should be taken into account when chemical potential oscillations are relatively large, which may be the case in extremely large fields, $\hbar\omega_c(B)\sim\varepsilon_F$.

Using Eq. (7) we obtain the component of the magnetization along magnetic field:

$$\frac{M(B)}{A}=\sum_{n=0}^{\bar{n}-1}\left(\zeta-\varepsilon_n-B\frac{\partial\varepsilon_n}{\partial B}\right)-B\frac{\partial\varepsilon_n^-}{\partial B}g(x,Q)$$
$$+(1/\beta)f(x,Q)-\hbar\omega_c h(x,Q),$$
$$h(x,Q)\equiv\sum_{k=1}^{\bar{n}}\frac{k[\cosh x+\exp(-kQ)]}{\cosh x+\cosh(kQ)}.\qquad(16)$$

Performing the summation in the first term of Eq. (16) over the Landau levels lying below the Fermi energy, we obtain

$$\sum_{n=0}^{\bar{n}-1}\left(\varepsilon_n+B\frac{\partial\varepsilon_n}{\partial B}\right)=2\sum_{n=0}^{\bar{n}-1}\varepsilon_n=\bar{n}^2\hbar\omega_c(B)=\bar{n}\varepsilon_F\left(1+\frac{b}{B}\right).\qquad(17)$$

The term in Eq. (16) containing the function $g(x,Q)$ can be written with the help of the equation for the chemical potential, Eq. (14), as

$$-\varepsilon_n^-(B)g(x,Q)=\left(\varepsilon_F+\frac{\hbar\omega_c(B_n^-)}{2}\right)\left(\frac{\varepsilon_F}{\hbar\omega_c(B_n^-)}\frac{b}{B_n^-}+\frac{c_R}{\hbar\omega_c(B_n^-)}\tilde{\zeta}\right).\qquad(18)$$

In deriving this expression we used the relations $F/B_n^-=\bar{n}=\varepsilon_F/\hbar\omega_c(B_n^-)$ and $\varepsilon_n^-(B)/B=\varepsilon_n^-(B_n^-)/B_n^-$.

Substituting Eqs. (17) and (18) into Eq. (16), we obtain for the magnetization in the fixed period $-2b_n^-\leqslant b\leqslant 0$

$$\frac{M(b)}{M_0}=\frac{2}{\hbar\omega_c(B_n^-)}\left[(1+c_R)\tilde{\zeta}(b)+\frac{\hbar\omega_c(B_n^-)}{2}\left(\frac{b}{B_n^-}+c_R\frac{\tilde{\zeta}(b)}{\varepsilon_F}+\frac{2k_BT}{\varepsilon_F}f(x,Q)-\frac{2\hbar\omega_c(B)}{\varepsilon_F}h(x,Q)\right)\right],\qquad(19)$$

where $M_0=\varepsilon_F\cos\Theta/\phi_0 c^*$ is the saturation magnetization at $T\to 0$. The second term in the large parentheses represents a small correction to the oscillating part of the magnetization and the first and last terms contribute to the uniform (diamagnetic) part (Landau diamagnetism). The first term in square brackets contains temperature dependence only through the chemical potential oscillations and remains finite

at $T\to 0$ [as in this case $\tilde{\zeta}(b\to 0,T\to 0)\to \hbar\omega_c/2$ (see Fig. 1)], while the terms in the large parentheses will be of the order $(\sim \hbar\omega_c/\varepsilon_F)$.

Thus, at temperatures and magnetic fields satisfying the conditions

$$k_B T \lesssim \hbar\omega_c(B)(Q\gtrsim 1), \quad \frac{2b_n^-}{B}\cong\frac{B}{F}=\frac{\hbar\omega_c(B)}{\varepsilon_F}\ll 1, \tag{20}$$

we obtain, to leading order in B/F, the general relation

$$\frac{M(b)}{M_0}=\frac{2}{\hbar\omega_c(B_n^-)}(1+c_R)\tilde{\zeta}(b). \tag{21}$$

Hence, *under the conditions represented by the expressions (20) the oscillating part of the magnetization is proportional to the oscillating part of the chemical potential. This result remains valid regardless of the presence of field independent (reservoir) states.*

Relation (21) was used in Ref. 12 for calculation of the magnetization for a canonical ensemble of electrons in closed electron orbits (i.e., for $c_R=0$ in the present model). It was shown there that the magnetic susceptibility $\partial M/\partial B$ at B_n^- and $\overline{B_n^-}$, where the LL spectrum has electron-hole symmetry (see Fig. 1), is proportional to the derivative of the oscillating part of the chemical potential:

$$\frac{1}{M_0}\frac{\partial M}{\partial B}\bigg|_{B_n^-,\overline{B_n^-}}=\frac{2}{\hbar\omega_c}\frac{\partial\tilde{\zeta}}{\partial B}\bigg|_{B_n^-,\overline{B_n^-}}. \tag{22}$$

In the more realistic model of the $(BEDT\text{-}TTF)_2X$ compounds studied here, the relevant closed orbits are situated in hole pockets of the Fermi surface. In this case the effective band mass is negative and the cyclotron mass is also negative, so that the wave form of the chemical potential oscillations is expected to be an inverse replica of the oscillations associated with electron orbits [in the sense that in the case of closed hole orbits an inversion of the chemical potential oscillation relative to the Fermi level should be made, $\tilde{\zeta}^{(h)}(b)=-\tilde{\zeta}(b)$, where $\tilde{\zeta}^{(h)}(b)$ is the chemical potential oscillations due to the closed hole orbits associated with a hole pocket of the Fermi surface and $\tilde{\zeta}(b)$ is the chemical potential oscillation due to the closed electron orbits associated with an electron pocket of the Fermi surface; see Fig. 1].

The relation between magnetization and the chemical potential oscillations for electrons moving in closed hole orbits and open electron orbits is

$$\frac{M(b)}{M_0}=\frac{2}{\hbar\omega_c(B_n^-)}(1+c_R)[-\tilde{\zeta}^{(h)}(b)]. \tag{23}$$

For a system consisting of a closed electron pocket and an open hole sheet the magnetization is given by the same expression as Eq. (21) but the transfer parameter is $c_R\sim|\partial p_{sh}/\partial\zeta|_{\varepsilon_F}$, where $\partial p_{sh}(\zeta)$ is the hole concentration in the hole sheet.

Hence, the shape of the magnetization oscillations is invariant relative to electrons moving on closed electron or hole orbits situated in the electron or hole pockets of the Fermi surface, the chemical potential oscillations due to closed hole orbits being antisymmetric (relative to the Fermi level) to those of closed electron orbits.

III. CHEMICAL POTENTIAL AND MAGNETIZATION OSCILLATIONS

In this section we will develop a parametric method of calculating the chemical potential and magnetization oscillations. All results will be shown to be valid irrespective of the mechanism of the electron transfer, i.e., for any reservoir of electrons filling either a continuous or a discrete field independent energy spectrum.

Instead of solving the complex transcendental equation for $\tilde{\zeta}(b)$ [see Eq. (14)], which cannot be solved analytically for arbitrary numbers of levels in all regions of the parameter $Q\gtrsim 1$ (see also Ref. 9, where it was solved for two levels and is therefore applicable for $Q\gtrsim 10$), we will try to solve it parametrically. We express the variable x from Eq. (5) by using the condition $b_n^-\ll B_n^-$ [which is equivalent to the conditions expressed in Eqs. (20)] in the form

$$\frac{2}{Q}x=1+\frac{b}{b_n^-}-\frac{2}{\hbar\omega_c}\tilde{\zeta}(b). \tag{24}$$

Solving Eqs. (14) and (24) for $\tilde{\zeta}$ and b/b_n^-, they can be written as explicit functions of x (which will serve here as the parametric variable), i.e.,

$$\frac{2}{\hbar\omega_c}\tilde{\zeta}(x)=\frac{1}{1+c_R}\left(1-2g(x,Q)-\frac{2}{Q}x\right),$$

$$-\frac{b(x)}{b_n^-}\equiv-\frac{k_n^- b(x)}{\pi}=\frac{2}{1+c_R}\left[g(x,Q)+\frac{c_R}{2}\left(1-\frac{2}{Q}x\right)\right]. \tag{25}$$

Varying x in the interval corresponding to the separated fixed period (see Fig. 1),

$$-\frac{Q}{2}\leqslant x\leqslant\frac{Q}{2}, \tag{26}$$

we obtain an explicit solution for the oscillating part of the chemical potential $\tilde{\zeta}(b)$ as a function of magnetic field in the separated quasiperiod $-2b_n^-\leqslant b\leqslant 0$ (see the left period relative to the fixed magnetic field B_n^- in Fig. 1).

As seen from the Eqs. (25) and the condition (26) (see Fig. 1), the solution is determined by the key dimensionless parameter Q, which reflects the combined influence of the magnetic field and temperature {for numerical estimates the relation $Q\cong[1.34B(\mathrm{T})]/(m_c/m_e)[T(\mathrm{K})]$ is useful}, and the transfer parameter c_R. It is seen that a finite value of c_R significantly suppresses the chemical potential oscillations at all Q: from Eqs. (25) it follows that at $c_R\gg 1$ the oscillating part of the chemical potential $\tilde{\zeta}\to 0$ at all magnetic fields inside the period $-2b_n^-\leqslant b\leqslant 0$.

Chemical potential oscillations for various transfer parameters c_R are shown in Fig. 2. It is seen that at $c_R\sim 1$ the chemical potential oscillation are symmetrized, whereas for $c_R\gtrsim 10$ they are almost completely suppressed. It will be shown in what follows that magnetization oscillations ampli-

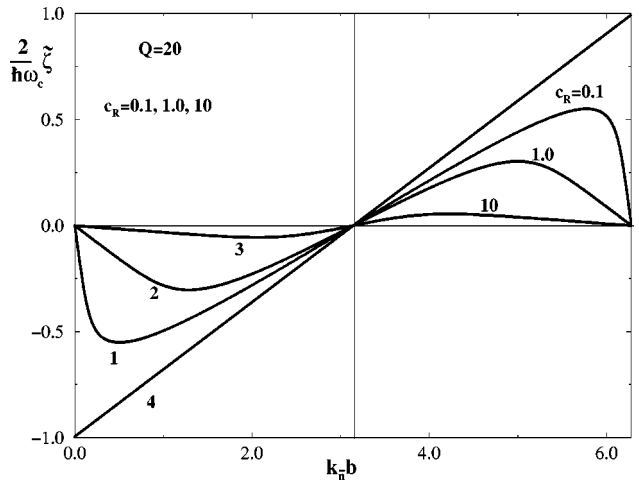

FIG. 2. Suppression of the chemical potential oscillations by equilibrium electron transfer. Curves 1, 2, and 3 are calculated according to the parametric Eqs. (25) and (26) for corresponding transfer constants $c_R=0.1$, 1.0, and 10, and for a fixed value of $Q \equiv \hbar\omega_c/k_BT=20$. Curve 4 is the level $\varepsilon_{\bar{n}}(b)$, that is, $[\varepsilon_{\bar{n}}(b)-\varepsilon_F]/\hbar\omega_c(B_{\bar{n}})/2$, crossing the chemical potential in the separated period. The three-level approximation, used here (and in calculations of oscillation curves in Figs. 3–6 below), yields a very accurate shape of the chemical potential oscillations. Here and also in the subsequent Figs. 3–6 a period shifted by 2π relative to the period chosen in Fig. 1 will be used: $0 \geqslant k_{\bar{n}}b \geqslant 2\pi$.

tudes are independent of the transfer parameter c_R, the shape of the oscillations being greatly influenced by this transfer, however.

Thermal smoothing of the chemical potential oscillations is shown for the canonical ensemble in Fig. 3 and for the grand canonical ensemble in Fig. 4. Note the symmetrical and sawtooth shapes at very low temperatures obtained in the presence and the absence of electron transfer, respectively.

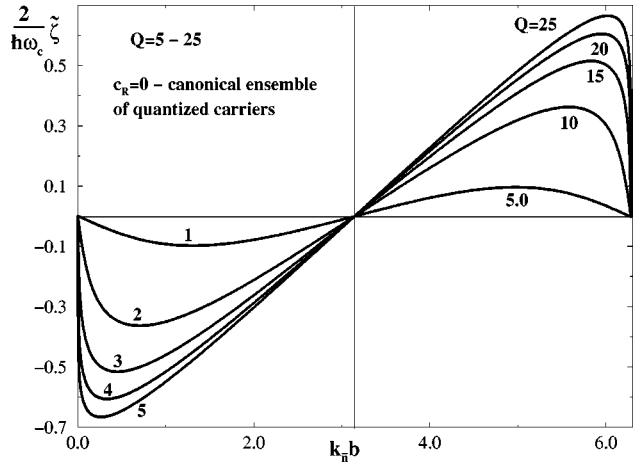

FIG. 3. Wave form of the chemical potential and magnetization oscillations in a metal without open parts of the Fermi surface and/or localized states, $c_R=0$. Curves, drawn according to the parametric Eqs. (25) and (26) (in the three-level approximation), can be interpreted as taken at different temperatures for fixed magnetic field (or at different fields for fixed temperature) corresponding to the values of the key parameter $Q=5-25$. Note the nearly sawtooth shape of oscillations at large Q (i.e., $Q=10-25$) and nearly symmetrical form of the oscillations in the high temperature–low magnetic field region, $Q \lesssim 5$. Note that according to Eq. (37) the magnetization oscillations in this case [namely, $M(b)/M_0$] are also presented by this drawing.

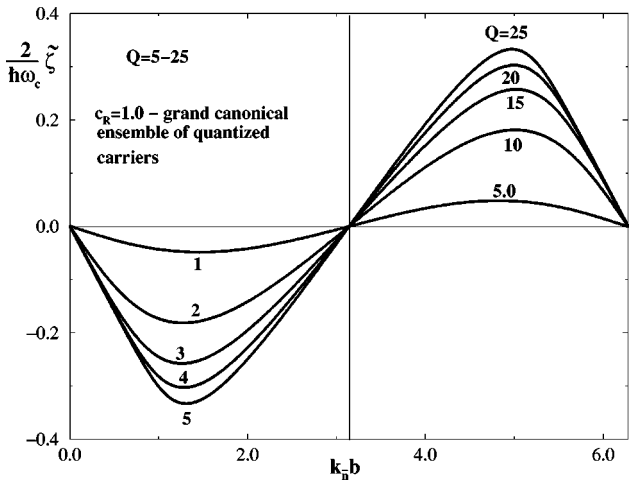

FIG. 4. Wave form of the chemical potential oscillations in a 2D metal in the presence of an electron reservoir (open parts of the Fermi surface and/or localized states). Curves are calculated according to the parametric Eqs. (25) and (26) (in the three-level approximation) with $c_R=1$ for various values of the parameter $Q=5-25$. These curves show oscillations smearing with increasing temperature (at fixed magnetic field) or with decreasing magnetic field (at fixed temperature). Note the symmetrical form of the oscillations at large $Q=10-25$, i.e., at low temperatures for fixed magnetic field (for comparison see Fig. 3, where chemical potential and magnetization oscillations have a strongly asymmetrical shape in the absence of open parts of the Fermi surface and/or localized states).

The magnetization can also be calculated via a parametric method in which only the function $g(x,Q)$ [Eq. (11)] needs to be calculated. The advantage of this method for 2D metals is that it allows one to sum over an arbitrary number of levels around the chemical potential and in this way to get an exact solution in the entire temperature–magnetic field range for an arbitrary $Q \equiv \hbar\omega_c/k_BT \gtrsim 1$. As will be shown later, except for the high temperature–low magnetic field region ($Q<5$), a single term in this sum is sufficient to get very accurate results. [In this approach only three levels around the Fermi energy are taken into account (three-level approximation).]

Some general relations for the magnetization can be obtained without explicitly calculating the function $g(x,Q)$ in a fixed quasiperiod. The magnetization, as it should be, is explicitly independent of the transfer parameter c_R, but depends on the parametric variable x, since magnetization is determined only by the electrons in the quantized orbits [see Eq. (16)]. Substituting the expression for the chemical potential [first of Eqs. (25)] into the expression for the magnetization, Eq. (21), we obtain

$$\frac{M(x)}{M_0}=1-2g(x,Q)-\frac{2}{Q}x. \tag{27}$$

The magnetic field values at which the magnetization is extremal (e.g., maximal at the magnetic field b_m) are the same as those where the chemical potential is extremal, and

are determined by the condition $\partial\tilde{\zeta}(b)/\partial b|_{b_m}=0$. Differentiating Eqs. (24) and (14) with respect to b and taking them at the maximal points, we obtain an equation for the corresponding value of the parametric variable $x_m \equiv x(b_m)$, i.e.,

$$\left.\frac{\partial x}{\partial b}\right|_{b_m}=\frac{Q}{2b_n^-},$$

$$\frac{1}{Q}=-\left.\frac{\partial g(x,Q)}{\partial x}\right|_{x_m}. \tag{28}$$

Using Eq. (11) we have

$$-\frac{\partial g(x,Q)}{\partial x}=\frac{1}{2(1+\cosh x)}+\sum_{k=1}^{\bar{n}}\left(\frac{1}{2[1+\cosh(kQ+x)]}+\frac{1}{2[1+\cosh(kQ-x)]}\right). \tag{29}$$

Note that the value of the parametric variable x_m can be obtained from the last equations, which are independent of the transfer parameter c_R.

Hence, the magnetization amplitude $M(x_m)$ obtained from Eq. (27) is also independent of the transfer parameter. The connection between b_m and x_m is through the second of Eqs. (25). We see that the magnetic fields b_m at which the magnetization is extremal depend strongly on the transfer parameter c_R. *Thus, only the shape of the magnetization oscillations is influenced by the thermal transfer of electrons between closed and open parts of the Fermi surface (and/or localized states), the magnetization amplitudes being unchanged.* These results are illustrated in Fig. 5 for different values of the transfer parameter: $c_R=0.1$ for curve 1, 1.0 for curve 2, 10 for curve 3, and 100 for curve 4.

Noting that, according to Eqs. (28) and (29) the parametric variable at a maximum of the chemical potential and magnetization is a function of Q only, $x_m(Q)$, we obtain from Eqs. (25) the maximum position in the limit of almost pinned chemical potential ($c_R \gg 1$):

$$-\frac{b_m^{(pin)}}{b_n^-}\cong 1-\frac{2}{Q}x_m(Q), \tag{30}$$

and the corresponding limiting value of the amplitude of the chemical potential oscillations:

$$\frac{\tilde{\zeta}_m^{(pin)}}{\hbar\omega_c}\cong\frac{2}{c_R}\left[-g(x_m,Q)+\frac{1}{2}\left(1-\frac{2}{Q}x_m(Q)\right)\right], \tag{31}$$

where $\tilde{\zeta}_m^{(pin)}\equiv\tilde{\zeta}(b_m^{(pin)})$. From the last equation we see that the chemical potential oscillations are almost completely suppressed at large c_R, i.e., $\tilde{\zeta}(b)\to 0$ at $c_R\to\infty$ (see Fig. 2).

In the one-level approximation we obtain the following explicit solution for x_m [from Eqs. (28) and (29), neglecting all terms in the sums]:

$$x_m(Q)\cong\ln(Q-2), \tag{32}$$

and the corresponding value of the $g(x,Q)$ function is

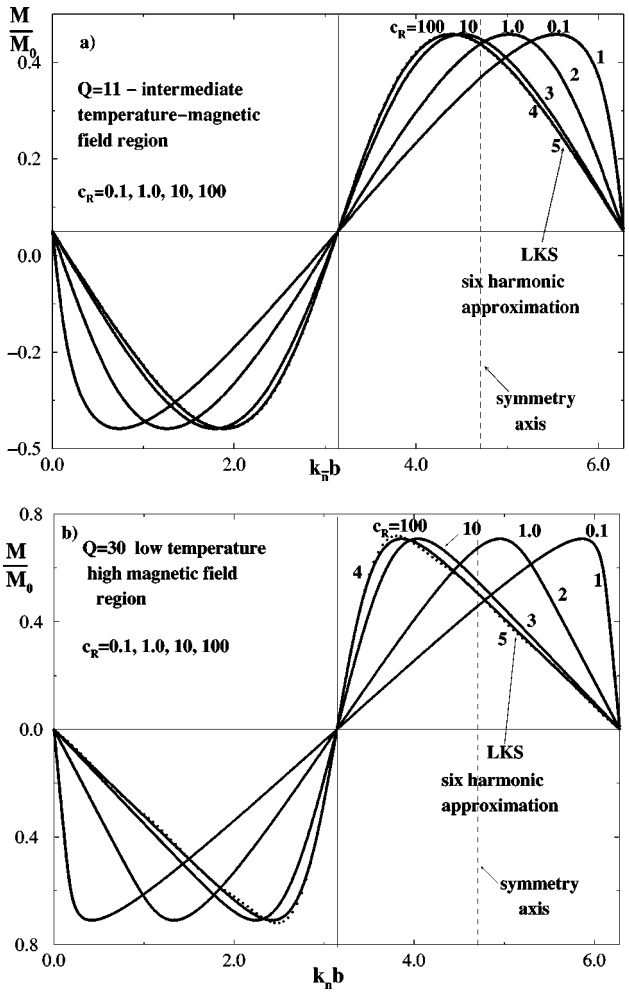

FIG. 5. Influence of equilibrium transfer of electrons between closed parts of the Fermi surface and reservoir (open orbits and/or localized states) on the magnetization oscillations in a 2D metal: (a) at intermediate temperature and magnetic fields, $Q=11$, and (b) at low temperature–high magnetic fields, $Q=30$. Magnetization oscillation curves are drawn according to the parametric Eqs. (25) and (26) and Eq. (21) for different transfer constant $c_R=0.1,1.0,10,100$ at fixed Q. (a) $Q=11$ (corresponding to parameters from Ref. 6, Fig. 2(b): $B=23$ T, $T=2.3$ K; effective cyclotron mass $m_c=1.2$ is taken from Ref. 8); (b) $Q=30$. Curves 1–4 are drawn in the level approximation (three-level approximation). Curves 5 [in (a) and (b), dotted curves] are drawn in the six-harmonic approximation of the Lifshitz-Kosevich-Shoenberg (LKS) 2D formula (see Ref. 10). Note the near coincidence of curves 3 and 4, obtained in the level approximation with large transfer constant $c_R=10,100$, at which the chemical potential oscillations are nearly suppressed (see Fig. 2, curve 3), with curve 5, obtained from the LKS formula for a 2D metal, derived in the case of complete suppression of the chemical potential oscillations. Note the symmetrization of the magnetization oscillations with increasing transfer of carriers (for $c_R\gtrsim 1$), the inverse-sawtooth wave form at $c_R\gg 1$, and the sawtooth wave form at $c_R\ll 1$. Note also the independence of the magnetization oscillation amplitude on electron transfer.

$$g(x_m,Q)\cong\frac{1}{Q-1}. \tag{33}$$

These expressions are independent of c_R and are valid for $Q\gtrsim 5$.

We can now obtain [using the second of Eqs. (25)] the positions of the magnetization maxima in two limiting cases. For a pinned chemical potential ($c_R \to \infty$),

$$-\frac{b_m^{(pin)}}{b_n^-} \cong 1 - \frac{2}{Q}\ln(Q-2), \tag{34}$$

and for a freely oscillating chemical potential ($c_R = 0$),[12]

$$-\frac{b_m^{(os)}}{b_n^-} = \frac{2}{Q-1}. \tag{35}$$

It is seen that in the case of a pinned chemical potential at very low temperatures ($Q \gg 1$) the magnetization maximum is shifted to the center of the period, $\overline{B_n^-}(b_m/b_n^- \to -1)$, i.e., we obtain the inverse-sawtooth wave form of oscillations observed in Ref. 6 [see Fig. 5(b), curves 3 and 4]. In the absence of any reservoir ($c_R \to 0$) at $Q \gg 1$ the maximum is shifted to the right edge of the period, B_n^-, i.e., we obtain the sawtooth wave form of oscillations observed in Ref. 5 [see Fig. 5(b), curve 1].

Note that the deviation of the maximum positions from the limiting values of the magnetic fields in the positive half-period is different in the two extreme cases $c_R \to \infty$ and $c_R \to 0$. For the same temperature and magnetic field (fixed Q) the maximum at $c_R \to \infty$ [see Eq. (34)] shifts farther from the center of period than the maximum at $c_R \to 0$ [see Eq. (35)] from the right end of the period. This reflects the fact that at fixed Q the sawtooth shape characteristic of a freely oscillating chemical potential is more pronounced than the inverse-sawtooth wave form characteristic of the pinned chemical potential.

An explicit solution for the magnetization as a function of magnetic field, $M(b)$, can be obtained only for a completely pinned chemical potential [$c_R \to \infty$, $\tilde{\zeta}(b) \to 0$]. In this case the parametric variable can be found as an explicit function of the magnetic field. Then a substitution of this $x(b)$ [found from Eq. (24) at $\tilde{\zeta} = 0$] into the expression for magnetization [Eq. (27)] solves the problem explicitly inside the period $-2b_n^- \leqslant b \leqslant 0$:

$$\frac{M^{(pin)}(b)}{M_0} = -\frac{b}{b_n^-} - 2g(x,Q), \quad x(b) = \frac{Q}{2}\left(1 + \frac{b}{b_n^-}\right). \tag{36}$$

This is the level approximation analog of the Lifshitz-Kosevich-Shoenberg formula for a 2D metal,[10] the latter containing all harmonics with the chemical potential replaced by the Fermi energy, i.e., with the chemical potential oscillations completely neglected [see Figs. 5(a) and 5(b), curves 5].

It should be noted that even in the case of completely suppressed chemical potential oscillations the magnetization oscillations retain their amplitudes, their shape being drastically changed compared to those of freely oscillating chemical potentials.

Magnetization oscillations in the absence of the electronic reservoir (i.e., for $c_R = 0$) are shown in Fig. 3. As expected,

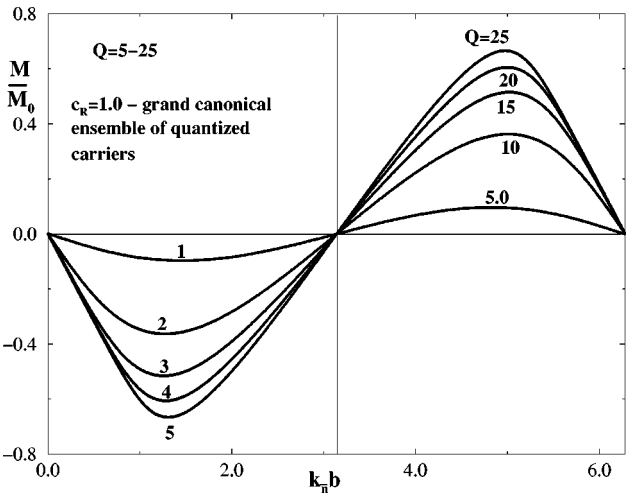

FIG. 6. Wave form of the magnetization oscillations in a metal with electron reservoir of field independent states for different temperatures (at fixed magnetic field) or for different magnetic fields (at fixed temperature). Curves are drawn according to the parametric Eqs. (25) and (26) (in three-level approximation) and Eq. (21) for $c_R = 1$ and different values of the parameter $Q = 5$–25. Note the nearly symmetric shape of the magnetization oscillations at $c_R = 1$ compared with the strongly asymmetric magnetization oscillations [Fig. 3, right-hand side sawtooth shape (at low temperatures or high magnetic fields)] in the absence of electron transfer, $c_R = 0$ and at large transfer, $c_R \gg 1$ [see Fig. 5(b), curves 3 and 4, left-hand side inverse-sawtooth shape]. The wave forms shown closely resemble the tendency to retain symmetrical forms of magnetization oscillation on lowering temperature observed in Refs. 8 and 7.

the magnetization oscillations in this case have a sawtooth shape at low temperature (large $Q \gtrsim 10$). In this case the general relation holds:

$$\frac{M(b)}{M_0} = \frac{2}{\hbar\omega_c}\tilde{\zeta}(b). \tag{37}$$

This follows from Eqs. (24) and (27) at $-b/b_n^- = 2g(x,Q)$, which is the equation for the chemical potential oscillations in the absence of electron transfer [see Eq. (14) with $c_R = 0$ and Ref. 12: $(2/\hbar\omega_c)\tilde{\zeta} = 1 + b/b_n^- - (2/Q)x = 1 - 2g(x,Q) - (2/Q)x = M(b)/M_0$]. A relation similar to Eq. (37) holds for electrons on closed hole orbits (hole pockets of the Fermi surface), but the substitution $\tilde{\zeta}(b) \to -\tilde{\zeta}^{(h)}(b)$ should be made.

Magnetization oscillations in the presence of a quasiplanar Fermi surface sheet and/or localized states are shown in Fig. 6. We see the almost symmetrical wave form of magnetization oscillations for $c_R = 1$ even at $T \to 0$ (large Q at fixed magnetic field). At larger $c_R \gtrsim 10$ the magnetization maximum shifts to the left and at small temperatures the oscillations have the inverse-sawtooth shape [see Fig. 5(b), curves 3 and 4].

IV. TRANSFER PARAMETER AND COMPARISON WITH EXPERIMENT

To compare the predictions of our model to the available experimental data in organic metals let us estimate the value of the transfer parameter for a specific situation. Such a two-

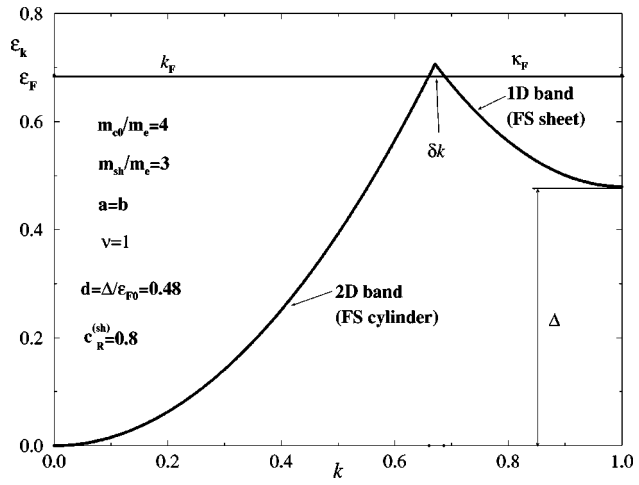

FIG. 7. A simple band structure model of the electronic energy near the cylindrical and planar Fermi surface (FS) sheets forming an energy barrier above the Fermi energy. Energies are measured in units of the Fermi energy ε_{F0} in the absence of a planar sheet, $\varepsilon \rightarrow \varepsilon/\varepsilon_{F0}$, etc. Wave vector components in the k_y direction are in π/b units; $k \rightarrow k/(\pi/b)$, etc., and masses are in electron mass units m_e. k_F is the k_y component of the Fermi vector of the FS cylinder, κ_F is the half width of the FS planar sheet (the Fermi vector of the sheet is measured from the Brillouin zone edge corresponding to $k=\pi/b$), and δk is the barrier width. Energies are measured from the bottom of the subband corresponding to the cylindrical energy surfaces. ε_F is the Fermi energy and Δ is the energy separation between the bottoms of the corresponding 2D and 1D conduction subbands. Here and in the subsequent Fig. 9 the isotropic case in the a-b plane is shown with the number of electrons in a unit cell $\nu=1$. The transfer constant calculated for the parameters used here is $c_R^{(sh)}=0.8$.

band model was considered by us in Ref. 12, where the two bands are nearly intersecting along one of the directions in k space. This direction was chosen along the **b** axis. The unit cell vectors **a**, **b**, and **c*** are supposed to be perpendicular to each other, **c*** being the unit cell vector in the anisotropic direction (**a** and **b** form the conducting plane in the organic metals[2]). The Brillouin zone in this case is approximated as a rectangle with dimensions $2\pi/a$, $2\pi/b$, and $2\pi/c^*$ where $a=|\mathbf{a}|$, $b=|\mathbf{b}|$, and $c^*=|\mathbf{c}^*|$ are the lattice constants in the corresponding directions.

The two highest occupied energy bands are assumed to overlap so as to form a gap in k space along the **b** axis (i.e., the k_y direction) between the cylindrical and planar Fermi surface sheets (see Fig. 7). Note the energy barrier created in this model between the two separated Fermi surface sheets, which does not appropriately describe the actual band structure of the materials studied. This discrepancy is not expected to lead to any serious problem, however, since the equilibrium transfer process is independent of the presence of such a barrier.

The dispersion of the electron energy in both sheets is assumed to be parabolic. For the planar sheets the 1D dispersion is in the k_y direction with effective mass m_{sh}. In the cylinder the dispersion is in the k_x and k_y directions with effective masses m_x and m_y, respectively (we take into account the anisotropy in the a-b plane when considering the elliptical Fermi surface cylinder). Here the ideal case of a 2D metal is considered, and hence the dispersion in the k_z direction (along **c***) is completely neglected.

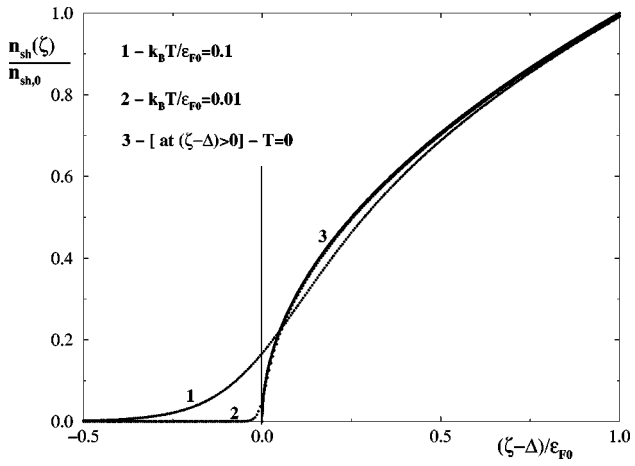

FIG. 8. Concentration of electrons in the 1D subband vs chemical potential. Curves 1 and 2 are drawn according to the exact formula Eq. (38): $k_BT/\varepsilon_{F0}=0.1$ for curve 1 and 0.01 for curve 2. Curve 3 is drawn according to the approximate formula Eq. (39) corresponding to the limit $T=0$. Note the maximal value of the derivative $\partial n_{sh}(\zeta)/\partial\zeta$ at $\zeta-\Delta=0$, due to the van Hove singularity in the 1D density of states, and the degenerate $[(\zeta-\Delta)>0]$ and nondegenerate $[(\zeta-\Delta)<0]$ regions for carriers filling the 1D subband. Note that at finite temperature this derivative is always finite, becoming extremely large at $T\rightarrow 0$.

The density of electrons filling the continuous (reservoir) spectrum can be written as

$$n_R^{(sh)}(\zeta)\equiv n_{sh}(\zeta)=\frac{1}{2v\sqrt{\varepsilon_{sh}}}\int_0^\infty [1+\exp(\varepsilon+\Delta-\zeta)\beta]^{-1}\frac{d\varepsilon}{\sqrt{\varepsilon}}, \tag{38}$$

where Δ is the energy difference between the bottoms of the two subbands (see Fig. 7), ζ is the chemical potential measured from the bottom of the band corresponding to the closed orbits, $\varepsilon_{sh}\equiv\hbar^2(\pi/b)^2/2m_{sh}$ is the bandwidth around the planar sheet, and $v=abc^*$ is the unit cell volume. At magnetic fields where $\zeta(B)=\varepsilon_F+\tilde{\zeta}(B)=\varepsilon_F$ the chemical potential coincides with the zero field value ε_F. This function, Eq. (38), is shown in Fig. 8.

In the degenerate case, where $(\zeta-\Delta)\gg k_BT$, the density of electrons filling the quasi-1D subband and moving in the magnetic field in open orbits is

$$n_{sh}(\zeta)=n_{sh,0}\left(\frac{\zeta-\Delta}{\varepsilon_{F0}}\right)^{1/2}, \quad n_{sh,0}\equiv\frac{1}{v}\sqrt{\frac{\varepsilon_{F0}}{\varepsilon_{sh}}}, \tag{39}$$

where ε_{F0} is the Fermi energy in the absence of this subband (see below). Equation (12) determining the Fermi energy can be written as

$$n_c=\frac{2}{c^*\phi_0\mu_{c0}}\varepsilon_F+n_{sh}(\varepsilon_F), \tag{40}$$

where $\mu_{c0}\equiv e\hbar/m_{c0}c$ and $m_{c0}=\sqrt{m_xm_y}$ is the cyclotron mass at $\Theta=0$.

The total electron density is field independent, $n_c=\nu/v$, where ν is the number of valence electrons per unit cell. We consider for definiteness the case of a half-filled Brillouin

zone, that is, the number of valence electrons in a unit cell is $\nu=1$. Introducing the Fermi energy in the absence of the continuous subband, $\varepsilon_{F0}=n_c c^* \phi_0 \mu_{c0}/2=\pi\nu\hbar^2/m_{c0}ab$, we obtain the solution of Eq. (40) for the Fermi energy in the degenerate case [Eq. (39)],

$$e_F \equiv \frac{\varepsilon_F}{\varepsilon_{F0}} = \tfrac{1}{2}[(e_{sh}+2)-\sqrt{e_{sh}^2+4e_{sh}(1-d)}], \qquad (41)$$

where $e_{sh}\equiv\varepsilon_{sh}/\varepsilon_{F0}=(2/\pi\nu)(m_{sh}/m_{c0})(b/a)$ is a reduced characteristic energy for the continuous subband and $d \equiv\Delta/\varepsilon_{F0}$ is the parameter characterizing the separation between the bottoms of the two subbands (see Fig. 7). Taking into account that the effective mass in the k_y direction is $m_y=m_{c0}/\sqrt{b/a}$ (assuming that $m_x/m_y=b/a$), we can determine the width of the energy barrier at the Fermi surface (in units of π/b), i.e., the gap in k space between the two Fermi surface sheets (see Fig. 7):

$$\delta k \equiv \delta k_y/(\pi/b)=1-(k_F+\kappa_F),$$

$$k_F \equiv \frac{k_{yF}}{\pi/b}=\left(\frac{2}{\pi}\nu\sqrt{\frac{b}{a}}e_F\right)^{1/2},$$

$$\kappa_F \equiv \frac{\kappa_{yF}}{\pi/b}=\left[\frac{2}{\pi}\left(\frac{b}{a}\right)\nu(e_F-d)\right]^{1/2}, \qquad (42)$$

where κ_F is the half width of the planar sheet in the k_y direction and $k_F\equiv k_{yF}$ is the Fermi vector component of the cylinder in this direction.

Now we can calculate the transfer parameter in the considered model. Using Eqs. (15), (10) and Eqs. (39), (41), we obtain

$$c_R^{(sh)}=\frac{1}{2}\frac{\sqrt{\varepsilon_{sh}}}{\sqrt{\varepsilon_F-\Delta}}$$

$$=\frac{1}{\sqrt{1+(2\pi/\nu)(m_{c0}/m_{sh})(a/b)(1-d)}-1}. \qquad (43)$$

It is seen that the transfer parameter, Eq. (43), significantly increases only for a very large ratio m_{sh}/m_e, when the 1D dispersion of the open energy surfaces is very weak and/or when the bottom of this 1D subband approaches the Fermi energy, i.e., for $d\to 1$ (see Fig. 9, curve 5). Note, however, that this enhancement occurs even if $(\zeta-\Delta)\gg k_BT$ [i.e., $(1-d)\gg k_BT/\varepsilon_{F0}$], that is, when the ''carriers'' filling the open energy surfaces are still degenerate and the approximation Eq. (39) is still valid [see Fig. 8, curve 3 at $(\zeta-\Delta)>0$].

In the special case when the bottom of the 1D subband is too close to the chemical potential, i.e., $|\zeta-\Delta|\lesssim k_BT$, we should analyze the situation with the help of the exact function Eq. (38) (see Fig. 8, curves 1 and 2). We see that the transfer parameter determined by Eq. (15) (here $c_R^{(sh)}\sim\partial n_{sh}/\partial\zeta$) can become maximal and very large in the case when the bottom of the 1D subband is situated near the Fermi energy (near $\zeta-\Delta=0$). This is due to the van Hove singularity of the density of states (DOS) at the 1D band edge [see Eq. (38)]. Note, however, that in this case the expansion of $n_{sh}(\zeta)$ in $\tilde{\zeta}$ [Eq. (10)] is valid as long as $\tilde{\zeta}$

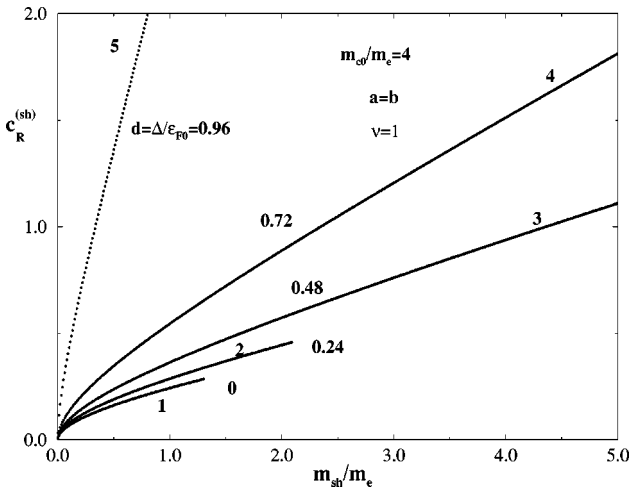

FIG. 9. Characteristic strength of the equilibrium transfer of electrons between closed and open sheets of the Fermi surface: transfer parameter vs effective mass of the 1D subband. Curves are calculated according to Eq. (43) at various separations between the bottoms of the 2D and 1D conduction subbands: $d=\Delta/\varepsilon_{F0}=0$ for curve 1; 0.24 for curve 2; 0.48 for curve 3; 0.72 for curve 4; 0.96 for curve 5. Effective mass is in electron mass units. Curves 1 and 2 are drawn up to the point where the barrier width between the cylindrical and the planar sheets vanishes, $\delta k=0$ (see Fig. 7). Note the large values of the transfer parameter for shallow 1D subbands (those having large effective mass) with the bottom of the 1D subband situated near the Fermi energy, $d=\Delta/\varepsilon_{F0}\lesssim 1$, curve 5.

$\ll k_BT$ (see Fig. 8, curves 1 and 2). Under these circumstances the value of the transfer parameter becomes temperature dependent and greatly increases with decreasing temperature [for estimating the derivative $\partial n_{sh}(\zeta)/\partial\zeta$, see Fig. 8, curves 1 and 2]. The chemical potential oscillations in this case are strongly suppressed ($\tilde{\zeta}\ll k_BT$), that is, the chemical potential is almost pinned to the large, field independent peak of the 1D DOS.

When the bottom of the 1D subband is above the chemical potential, $(\Delta-\zeta)>0$, the ''carriers'' enclosed by the planar sheets become nondegenerate, their concentration in the limit $(\Delta-\zeta)\gg k_BT$ is $n_{sh}(\zeta)\sim\exp[-(\Delta-\zeta)/k_BT]$ [see Fig. 8, curves 1 and 2 at $(\zeta-\Delta)<0$], and the transfer parameter $c_R^{(sh)}\sim\partial n_{sh}/\partial\zeta$ is greatly reduced.

Let us now discuss our results in connection with the available experimental data. The asymmetrical (inverse-sawtooth) shape of the magnetization oscillations observed in α-(BEDT-TTF)$_2$KHg(SCN)$_4$, as reported in Ref. 6, Fig. 2(b), is well described by our analytical formulas (see Fig. 5(a), curves 3 and 4) except at magnetic fields in the vicinity of the antiferromagnetic–normal metal phase transition, $B_K\sim$23–24 T, observed in this metal.[17,8] The wave form of the magnetization oscillations in the right part of Fig. 2(b) of Ref. 6 resembles our Fig. 5(a), curves 3 and 4, for $Q\cong 11$ [This value of Q corresponds to the data of the experiment reported in Ref. 6, Fig. 2(b): $B=23$ T, $T=2.3$ K with cyclotron mass near the above mentioned phase transition taken from Ref. 8: $m_c/m_e\cong 1.2$.] Curve 3 of Fig. 5(a) corresponds to $c_R=10$, curve 4 to $c_R=100$. Such large values for the transfer parameter may be obtained if the bottom of the 1D band is situated near the Fermi energy (see Fig. 9, curve 5), which is not the case for the pure limit of the material con-

sidered here.[2] The presence of an impurity with levels near the bottom of the 1D subband can lead to the situation where both the impurity level and the van Hove singularity will appear near the Fermi level, leading to large transfer of electrons and large values of the transfer parameter.

But even for such large values of the transfer parameter the extremely sharp inverse-sawtooth wave form seen in the left part of Fig. 2(b) of Ref. 6 (in the vicinity of the phase transition) cannot be explained for the experimental parameters given in Ref. 6, even with the cyclotron mass from Ref. 8. Thus in the framework of the model considered here only a drastic reduction of the cyclotron mass can lead to the observed inverse-sawtooth wave form of oscillations near the above mentioned phase transition. In Fig. 5(b), curves 3 and 4, which correspond to $Q=30$, the cyclotron mass should be reduced by nearly a factor of 3 (to obtain $Q=30$ instead of $Q=11$), so as to lead to the observed inverse-sawtooth shape of the magnetization oscillations.

It should be noted that spin splitting of Landau levels can also contribute to the change of the wave form of magnetization oscillations in 2D metals. In the material discussed, a clear spin-splitting structure is seen at very low temperature (in Ref. 8 at $T=0.48$ K). In the experiment reported in Ref. 6, the temperature was raised to $T=2.3$ K to avoid the appearance of the spin-split structure. According to our theoretical conditions for the appearance of the spin-split structure derived in Ref. 16, at the experimental parameters of the material discussed in the region of magnetic fields less than $B_K\sim 23$ T, such as the spin-splitting parameter $s=0.35$ (corresponding to the value $gm_c/m_e=4.70$ from Ref. 17) and $Q=11$, the spin-split structure is forbidden to appear. Hence, we can apply our approach neglecting the spin-splitting effect in this particular experimental case.

Another possible mechanism for shifting the maxima of the oscillations to the left, which could lead to an inverse-sawtooth-like-shape, is due to the effect of magnetic interaction.[1,18] The corresponding shift of the maximum to the left relative to the symmetrical position can be written as $\Delta h_e/b_n^{-}\equiv 4\pi(1-n_{dem})(M_0/b_n^{-})[M(x_m)/M_0]$, where $M_0/b_n^{-}=[(e^2/c^*)/\pi m_e c^2](F_0/B_n^{-})^2/(m_{c0}/m_e)$ (F_0 is the fundamental frequency at $\Theta=0$ and n_{dem} is the demagnetization factor). For the parameters of Ref. 6, Fig. 2(b), $F_0=674$ T, $B_n^{-}=23$ T, $T=2.3$ K, with $m_{c0}/m_e=1.2$ from Ref. 8 and $M(x_m)/M_0\sim 0.4$ [taken from our Fig. 5(a) ($Q=11$)], we find $\Delta h_e/b_n^{-}\sim 10^{-3}(1-n_{dem})$. The corresponding shift due to the presence of the planar Fermi surface sheet is $0.5-2\ln(Q-2)/Q\sim 10^{-1}$ for $Q=10$ [see Eq. (34)]. Hence, the influence of magnetic interaction on the shape of magnetization oscillations in the organic metal under study is negligible in comparison with the electron transfer mechanism discussed above.

Judging from the band structure of the considered organic metal without impurities the value of the transfer constant should be $c_R\sim 1$. Hence, a nearly symmetrical wave form of oscillations is predicted by our theory for this material, if relatively pure, down to the lowest temperature used (see Fig. 6), in agreement with the observed oscillations reported in Refs. 8 and 7. Our theoretical curve 2 from Fig. 5(b) well recalls the wave shape of experimental magnetization oscillations obtained for the discussed material in its metallic phase at magnetic field $B\sim 27$ T and temperature $T\sim 0.5$ K by Honold *et al.*[19] [see Fig. 2(b) from Ref. 19]. For the experiment of Ref. 19, we get for the metallic phase the value for the parameter $Q\sim 36$ ($B=27$ T, $T=0.5$ K, and $m_c/m_e\sim 2$), which together with the transfer parameter $c_R\sim 1$ gives an even better fit with the experimental curve.

Interesting experimental results concerning the wave shape of magnetoresistance oscillations, also including the quantized Hall effect, the magnetic breakdown effect, and the spin-splitting effect in organic 2D metals have appeared recently.[20–23] But their proper explanation, it seems, is beyond the scope of the theory proposed here for magnetization oscillations (dHvA effect). We hope to generalize our theory by taking such phenomena into consideration.

The different wave forms of magnetization oscillations reported for the same material may be attributed to the different purity of the samples used, which is expressed in terms of different Dingle temperatures. The possibility of equilibrium electron transfer between impurity levels and the extended 2D states could lead to more asymmetrical oscillation wave forms, especially in the case when the impurity levels are situated near the Fermi energy. This situation resembles the influence of the 1D van Hove singularity discussed above. The combined influence of both continuous and localized levels can lead to an inverse-sawtooth wave form of oscillations for materials with low cyclotron mass even at relatively high temperatures.

V. CONCLUSION

The influence of electrons occupying magnetic field independent energy levels [i.e., forming an effective reservoir of electrons on open sheets of the Fermi surface, or in localized impurity (defect) and intercalant states, etc.] on the magnetoquantum oscillations of the chemical potential and magnetization in a 2D metal has been investigated. It is shown quite generally that the magnetization oscillation wave form is a replica of the chemical potential oscillation pattern. They oscillate in phase if the quantized orbits are electronlike (i.e., there are electron pockets of the Fermi surface) and in antiphase if the orbits are holelike (i.e., there are hole pockets of the Fermi surface); hence, the wave form of magnetization oscillations is invariant relative to electrons moving in electron or hole orbits. It is also proved quite generally that equilibrium transfer of carriers between a reservoir of field independent states near the Fermi energy and the Landau levels influences only the shape (wave form) of the magnetization oscillations, the amplitude of the magnetization being unchanged.

The chemical potential oscillations are suppressed by sufficiently large transfer of carriers. In the case when the reservoir states correspond to an open quasiplanar sheet of the Fermi surface, a situation characterizing many of the organic conductors under study, the quasi-1D nature of the corresponding subband can lead to a large enhancement of this electron transfer. For near coincidence of the Fermi energy with the bottom of the quasi-1D subband, the chemical potential is pinned to the corresponding van Hove singularity at the band edge, leading to extreme left-handed asymmetry of the magnetization oscillation wave form at sufficiently low temperatures (inverse-sawtooth shape).

The opposite limit, $c_R\ll 1$, for which the magnetization

oscillations have at $T \to 0$ the right-handed sawtooth shape (see Ref. 9), corresponds to a broader range of the relevant band structure parameters, and so within the present model it is expected to be a more common phenomenon. This ideal (canonical ensemble) situation is, however, very sensitive to the presence of extrinsic types of electron reservoir, such as intercalant or impurity (defect) states,[11] which could lead to the symmetrization of magnetization oscillations.

The typical transfer constant for the quasi-2D organic metals (BEDT-TTF)$_2X$, which is $c_R \lesssim 2$, leads to only partial suppression of the chemical potential oscillations, but is in the range where the shape of the magnetization oscillation is nearly symmetrical at all temperatures. The transfer parameter is larger for open 1D bands with effective mass $m_{sh} > m_e$, i.e., for shallower sheets with bottom nearer to the Fermi energy. For such materials more asymmetrical oscillations at low temperatures may be observed. The presence of impurity levels near the Fermi energy can also lead to this situation.

ACKNOWLEDGMENTS

Valuable discussions with A. Gordon are acknowledged. This research was supported by the German-Israeli Foundation for scientific research and development, Grant No. G-0456-220.07/95, and the Israel Science Foundation founded by the Israel Academy of Sciences and Humanities. The support of the Center for Absorption in Science, Ministry of Immigrant Absorption, State of Israel (Gil'adi Foundation) is also acknowledged.

[1] D. Shoenberg, *Magnetic Oscillations in Metals* (Cambridge University Press, Cambridge, 1984).
[2] J. Wosnitza, Int. J. Mod. Phys. B **7**, 2707 (1993); *Fermi Surfaces of Low-Dimensional Organic Metals and Superconductors* (Springer, Berlin, 1996).
[3] I.M. Lifshitz and A.M. Kosevich, Zh. Éksp. Teor. Fiz. **29**, 730 (1956) [Sov. Phys. JETP **2**, 636 (1956)].
[4] R. Peierls, Z. Phys. **81**, 186 (1933).
[5] M. Tokumoto, A.G. Swanson, J.S. Brooks, M. Tamura, H. Tajima, and H. Kuroda, Solid State Commun. **75**, 439 (1990).
[6] M. Tokumoto, A.G. Swanson, J.S. Brooks, C.C. Agosta, S.T. Hannahs, N. Kinoshita, H. Anzai, M. Tamura, H. Tajima, H. Kuroda, A. Ugawa, and K. Yakushi, Physica B **184**, 508 (1993).
[7] J.S. Brooks, P. Sandhu, J.S. Qualls, S. Hill, and M. Tokumoto, Physica B **246-247**, 307 (1998).
[8] S. Uji, J.S. Brooks, M. Chaparala, L. Seger, T. Szabo, M. Tokumoto, N. Kinoshita, T. Kinoshita, Y. Tanaka, and H. Anzai, Solid State Commun. **100**, 825 (1996).
[9] I.D. Vagner, T. Maniv, and E. Ehrenfreund, Phys. Rev. Lett. **51**, 1700 (1983).
[10] D. Shoenberg, J. Low Temp. Phys. **56**, 417 (1984).
[11] I.D. Vagner, T. Maniv, W. Joss, J.M. van Ruitenbeck, and K. Jauregui, Synth. Met. **34**, 393 (1989).
[12] M.A. Itskovsky, T. Maniv, and I.D. Vagner, Z. Phys. B: Condens. Matter **101**, 13 (1996).
[13] N. Harrison, R. Bogaerts, P.H.P. Reinders, J. Singleton, S.J. Blundell, and F. Gerlach, Phys. Rev. B **54**, 9977 (1996).
[14] A.S. Alexandrov and A.M. Bratkovsky, Phys. Rev. Lett. **76**, 1308 (1996).
[15] E. Lifshitz and L. Pitaevsky, *Statistical Physics* (Pergamon, Oxford, 1986), Pt. 2.
[16] M.A. Itskovsky, S. Askenazy, T. Maniv, I.D. Vagner, E. Balthes, and D. Schweitzer, Phys. Rev. B **58**, R13 347 (1998).
[17] T. Sasaki and T. Fukase, Phys. Rev. B **59**, 13 872 (1999).
[18] M.A. Itskovsky, G.F. Kventsel, and T. Maniv, Phys. Rev. B **50**, 6779 (1994).
[19] M.M. Honold, N. Harrison, J. Singleton, H. Yaguchi, C. Mielke, D. Rickel, I. Deckers, P.H.P. Reinders, F. Herlach, M. Kurmoo, and P. Day, J. Phys.: Condens. Matter **9**, L533 (1997).
[20] N. Harrison, A. House, M.V. Kartsovnik, A.V. Polisski, J. Singleton, F. Herlach, W. Hayes, and N.D. Kushch, Phys. Rev. Lett. **77**, 1576 (1996).
[21] M.M. Honold, N. Harrison, M.-S. Nam, J. Singleton, C.H. Mielke, M. Kurmoo, and P. Day, Phys. Rev. B **58**, 7560 (1998).
[22] N. Harrison, C.H. Mielke, D.G. Rickel, J. Wosnitza, J.S. Qualls, J.S. Brooks, E. Balthes, D. Schweitzer, I. Heinen, and W. Strunz, Phys. Rev. B **58**, 10 248 (1998).
[23] M.M. Honold, N. Harrison, J. Singleton, M.-S. Nam, S.J. Blundell, C.H. Mielke, M.V. Kartsovnik, and N.D. Kushch, Phys. Rev. B **59**, R10 417 (1999).